Astron. Astrophys. 181, 71–76 (1987)

ASTRONOMY AND ASTROPHYSICS

Some physical processes influencing the polarization of continuum and line radiation

K.N. Nagendra and A. Peraiah

Indian Institute of Astrophysics, Bangalore 560034, India

Received June 5, 1985; accepted January 5, 1987

Summary. Some physical mechanisms which affect the continuum and line polarization are studied. The physical conditions of the plasma selected for this purpose represent different astrophysical situations of interest, particularly the magnetic stars. The pure absorption polarization transfer equation is solved individually taking these effects into account.

Key words: polarization – magnetic field – plasmas- radiative transfer

1. Introduction

The analysis of polarimetric observations requires in certain cases the solution of the transfer problem taking account of relevant physical mechanisms. The basic theory of polarization radiative transfer (see Stenflo, 1971 and references therein) is used for this purpose. In the following sections we have attempted to study the impact of certain physical processes on the conventional solutions, which are negligible in the first approximation, but produce significant changes in the intensity and polarization of emitted radiation under specific conditions of interest.

2. The Stark effect in the presence of a strong magnetic field

The Stark and Zeeman effects are equally important in computing the hydrogen line profiles in moderately strong magnetic fields, where the Zeeman or Paschen Back effects are not too dominant over the Stark effects. Nguyen-Hoe et al. (1967) calculated the Stark 'profile functions' in a magnetic field using the impact approximation. Recently, in a series of papers, Mathys (1983, 1984a,b and 1985a) has developed a more accurate unified theory and computed the profile functions for a wide range of temperatures (T_e), electron densities (N_e) and magnetic fields (B). The unified theory approach for the non-magnetic Stark profiles is given by Smith et al. (1969); Vidal et al. (1970, 1971). The modification of the unified theory to include ion dynamical effects is presented in Cooper et al. (1974). The hydrogen line broadening is primarily caused by a strong linear Stark effect due to interactions between the radiating atom or ion and local electric microfields produced by perturbing ions and electrons. When an external magnetic field is present, such as to act only as an additional perturbation, the classical straight line path approximation remains still valid. In a recent work Mathys (1984b) has included the ion dynamical effects also in the computation of Stark-Zeeman profiles. The Stark-Zeeman profiles cannot be obtained by simply convolving the non-magnetic Stark broadened profiles with pure Zeeman patterns, because the collisional transitions between the Zeeman substates of a given level cannot be neglected (Mathys, 1984b). Hence we have to use the magnetic field modified Stark profiles, and convolve them with a Doppler broadening function to obtain the required profile functions.

The theory of polarization radiative transfer for hydrogen line formation under the combined influence of Stark and Zeeman effects has been formulated by Mathys (1985b). We briefly describe the required equations and solve them to obtain the hydrogen line profiles formed in a realistic model atmosphere, for a given value of the magnetic field. The model atmosphere and the field strength represent the conditions typical of magnetic Ap stars. We use the radiative transfer formalism presented by Mathys (1985b). The transfer equation in LTE, for the polarized intensity $\mathbf{I} = (\mathrm{IQUV})^T$ is given by

$$\mu \frac{d\mathbf{I}}{d\tau} = \mathbf{AI} - \mathbf{S} \tag{1}$$

where, as usual $\mu = \cos\theta$, θ being the angle between the propagation and vertical (Z) directions. $\mathbf{A}$ and $\mathbf{S}$ are respectively the absorption matrix (transfer matrix) and the source vector, represented as

$$\mathbf{A} = \mathbf{1} + \mathbf{A}^L; \quad \mathbf{S} = \mathbf{J}B_\nu + \mathbf{S}^L, \tag{2}$$

where $\mathbf{1}$ is a (4×4) unit matrix and $\mathbf{J} = (1\,0\,0\,0)^T$. B_ν is the Planck function. $d\tau = -k^C \rho dZ$, k^C being the continuous absorption coefficient (in $\mathrm{cm}^2/\mathrm{gm}$) and ρ the mass density. The line absorption matrix $\mathbf{A}^L$ and the emission vector $\mathbf{S}^L$ are given as

$$\mathbf{A}^L = N'\mathbf{B}_{\mathrm{abs}} - N\mathbf{B}_{\mathrm{em}}; \quad \mathbf{S}^L = N\mathbf{E}, \tag{3}$$

where N and $N'(\mathrm{cm}^{-3})$ are respectively the populations of upper level n and the lower level n'. The stimulated emission matrix is given for a frequency ω by

$$\mathbf{B}_{\mathrm{em}} = \frac{2\pi^2\omega}{\hbar c}\left(\frac{\mathbf{b}_{\mathrm{em}}}{\rho k^c}\right). \tag{4}$$

The most general form of $\mathbf{b}_{\mathrm{em}}$ has been derived by Mathys (1985b). The $\mathbf{b}_{\mathrm{em}}$ in a restricted (zero azimuth; $\chi \equiv 0$) coordinate system

Send offprint requests to: K.N. Nagendra

is given as

$$(\mathbf{b}_{em})_0 = \begin{bmatrix} (1+\cos^2\psi)I_{xx} + \sin^2\psi I_{zz}; & \sin^2\psi(I_{zz}-I_{xx}); & 0; \\ 2\cos\psi R_{xx} & & \\ \sin^2\psi(I_{zz}-I_{xx}); & (1+\cos^2\psi)I_{xx} + \sin^2\psi I_{zz}; & \\ 2\cos\psi I_{xx}; & 0 & \\ 0; & -2\cos\psi I_{xx}; & (1+\cos^2\psi)I_{xx} + \sin^2\psi I_{zz}; \\ \sin^2\psi(R_{zz}-R_{xx}) & & \\ 2\cos\psi R_{xx}; & 0; & \sin^2\psi(R_{xx}-R_{zz}); \\ (1+\cos^2\psi)I_{xx} + \sin^2\psi I_{zz} & & \end{bmatrix} \tag{5}$$

The absorption matrix, in the same choice of coordinate system is given by

$$(\mathbf{b}_{abs})_0 = \begin{bmatrix} (1+\cos^2\psi)I'_{xx} + \sin^2\psi I'_{zz}; & \sin^2\psi(I'_{zz}-I'_{xx}); & 0; \\ 2\cos\psi R'_{xx} & & \\ \sin^2\psi(I'_{zz}-I'_{xx}); & (1+\cos^2\psi)I'_{xx} + \sin^2\psi I'_{zz}; & \\ -2\cos\psi I'_{xx}; & 0 & \\ 0; & 2\cos\psi I'_{xx}; & (1+\cos^2\psi)I'_{xx} + \sin^2\psi I'_{zz}; \\ \sin^2\psi(R'_{xx}-R'_{zz}); & & \\ 2\cos\psi R'_{xx}; & 0; & \sin^2\psi(R'_{zz}-R'_{xx}); \\ (1+\cos^2\psi)I'_{xx} + \sin^2\psi I'_{zz} & & \end{bmatrix} \tag{6}$$

where ψ is the angle between the propagation and field directions. We define

$$\left.\begin{aligned} I_{xx} &= \frac{\mathrm{Re}}{\pi} J_{xx} \\ R_{xx} &= \frac{-\mathrm{Im}}{\pi} J_{xx} \end{aligned}\right\}; \qquad \left.\begin{aligned} I_{zz} &= \frac{\mathrm{Re}}{\pi} J_{zz} \\ R_{zz} &= \frac{-\mathrm{Im}}{\pi} J_{zz} \end{aligned}\right\}, \tag{7}$$

with the emission profile functions defined as

$$\begin{aligned} J_{xx} &= i \sum_{\{ll'mm'\}} \langle \mathrm{n l_a m_a}|\rho_A|\mathrm{n l_a m_a}\rangle \\ &\times \langle \mathrm{n l_a m_a}|\mathbf{e_x}\cdot\mathbf{D}|\mathrm{n' l'_a m'_a}\rangle\langle \mathrm{n' l'_b m'_b}|\mathbf{e_x}\cdot\mathbf{D}|\mathrm{n l_b m_b}\rangle \\ &\times \langle \mathrm{n' l'_b m'_b};\, \mathrm{n l_b m_b}|[\Delta\omega - \mathscr{L}(\Delta\omega_0)]^{-1}|\mathrm{n l_a m_a};\, \mathrm{n' l'_a m'_a}\rangle . \end{aligned} \tag{8}$$

ρ_A and $\mathbf{D}$ are the density operator and the dipole momentum operator of the radiator. J_{zz} is obtained through replacing x by z. The computation of the last factor of the right-hand side of Eq. (8) has been described by Mathys (1984b). The absorption profile functions I'_{xx} etc. are defined in the same way as I_{xx} etc. from a quantity J'_{jk} $(j,k = x,z)$ identical to J_{jk} except for the change in density matrix element:

$$\langle \mathrm{n l_a m_a}|\rho_A|\mathrm{n l_a m_a}\rangle \rightarrow \langle \mathrm{n' l'_a m'_a}|\rho_A|\mathrm{n' l'_a m'_a}\rangle . \tag{9}$$

These density matrix elements are given by

$$\langle \mathrm{n l_a m_a}|\rho_A|\mathrm{n l_a m_a}\rangle = 1/n^2 , \tag{10}$$

for the emission profile function, and

$$\langle \mathrm{n' l'_a m'_a}|\rho_A|\mathrm{n' l'_a m'_a}\rangle = 1/n'^2 , \tag{11}$$

for the absorption profile function respectively. The populations of the levels n and n' can be obtained from the Saha-Boltzmann equation. The spontaneous emission vector E is given by

$$\mathbf{E} = \frac{2\hbar\omega^3}{(2\pi c)^2}\mathbf{B}_{em}\mathbf{J} . \tag{12}$$

The profile functions mentioned above are valid for a radiator at rest. The thermal motion of the radiators can be accounted for by convolving them with a Doppler broadening function as follows (Mihalas, 1978; Eq. 9.28)

$$\left.\begin{aligned} \bar{I}_{xx} \equiv \bar{I}_{xx}(\omega) &= \int_{-\infty}^{+\infty} I_{xx}\left(\omega - \frac{\zeta}{c}\omega\right) W(\zeta)d\zeta \\ \bar{R}_{xx} \equiv \bar{R}_{xx}(\omega) &= \int_{-\infty}^{+\infty} R_{xx}\left(\omega - \frac{\zeta}{c}\omega\right) W(\zeta)d\zeta \end{aligned}\right\}, \tag{13}$$

with

$$I_{xx}(\omega) = \frac{10^8\,\lambda^2}{2\pi c F_0} I_{xx}(\alpha); \qquad \alpha = \frac{\Delta\lambda(\text{Å})}{F_0}, \qquad F_0 = 2.61\,\mathrm{eN_e^{2/3}} . \tag{14}$$

There are two similar expressions for $\bar{I}_{zz}$ and $\bar{R}_{zz}$. We have employed $\bar{I}$ and $\bar{R}$ profiles instead of I and R, in computing the matrix elements of $(\mathbf{b}_{em})_0$. The elements of the absorption matrix $(\mathbf{b}_{abs})_0$ and the emission vector $\mathbf{E}$ are also computed using such Doppler broadened profile functions.

$$W(\zeta)d\zeta = \frac{1}{\sqrt{\pi}}\exp(-\zeta^2/\zeta_0^2)\frac{d\zeta}{\zeta_0}, \tag{15}$$

is the Maxwellian velocity distribution function which is the probability of finding an atom with an observer's frame line of sight velocity ζ in the range $(\zeta, \zeta + d\zeta)$. The thermal velocity of the atoms is $\zeta_0 = \sqrt{2kT/M}$. It is to be noted that the natural line broadening is always negligible compared to the Stark broadening, so that the Doppler convolved profiles represent a realistic situation in a dense hydrogen plasma.

In a magnetized plasma, the atoms moving in a magnetic field 'see' an electric field (a Lorentz electric field), whose contribution to the Stark broadening is not a priori negligible, for the outermost layers of the stellar atmosphere, though the contribution is quite small for lower field strengths ($B < 3$–$4\,10^4$ G) and higher densities ($N_e > 10^{14}\,\mathrm{cm^{-3}}$). Yet, the inclusion of this effect into the Stark-Zeeman profile function calculation would be rather difficult and time consuming, in view of the explicit velocity and angle dependence of this Lorentz electric field. We are grateful to Dr. G. Mathys for drawing our attention to this point through a personal communication.

For the computation of Hα line profile shown in Fig. 1, we have chosen a model atmosphere from Kurucz (1979) and employed a field strength of $B = 2\,10^4$ G. The I and R profiles were computed using the code kindly provided by Dr. Mathys, and then the convolution is performed to get $\bar{I}$ and $\bar{R}$. The method of solution of the transfer equation is described in Nagendra and Peraiah (1985a). The boundary condition used at $\tau = \tau_{max}$ is $I = (B_\nu 0\,0\,0)^T$. The depth integration of the transfer equation is stopped at $\tau_{max} \simeq 3.2$, in order to satisfy the requirement $N_e \lesssim 10^{15}\,\mathrm{cm^{-3}}$ needed to use the unified theory with ion dynamics in the profile function calculation. The lower limit of N_e is fixed by the condition $4.04\,10^{-3}\sqrt{N_e} \gtrsim B$ (straight line paths of the perturbers). Only half of the line is shown, since it is symmetric about the line centre. The importance of treating the hydrogen lines with an exact theoretical analysis employing the theory of combined Stark-Zeeman effect has been clearly demonstrated by Mathys (1984a, 1985b). We shall now see the usefulness of such a calculation when adopted into a realistic line formation problem. Since all the physical parameters are depth dependent, it is not easy to draw general conclusions using these results. How-

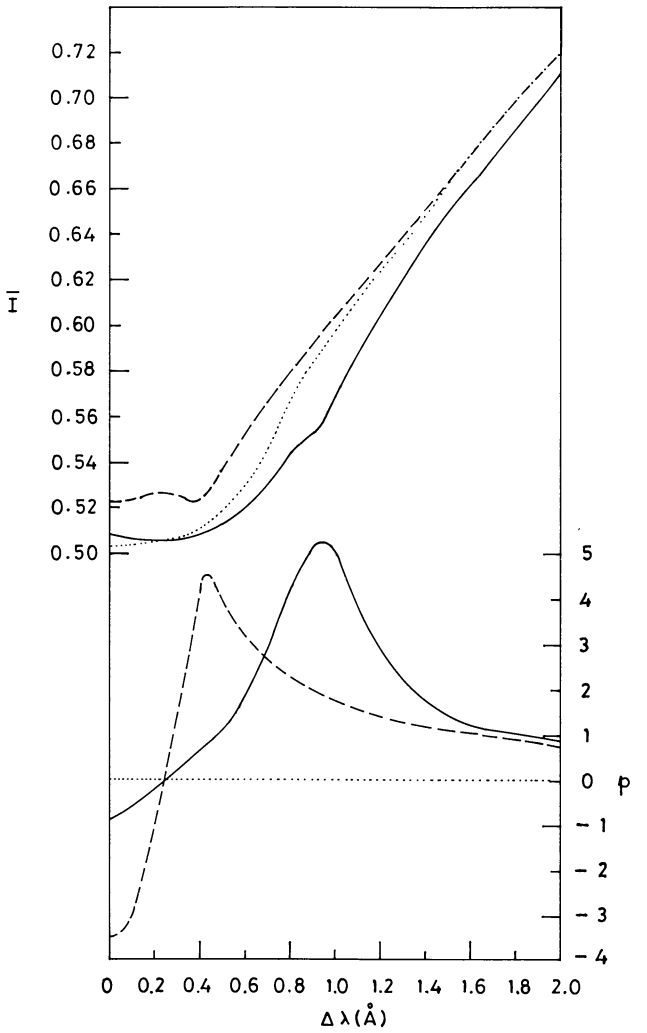

Fig. 1. Hα line profiles ($\lambda_0 = 6562.813$ Å) formed in a transverse magnetic field are shown. These realistic line profiles are computed using Mathy's formulation of the transfer equation, adopting a normal stellar atmospheric model given by Kurucz (1979), with $T_{\rm eff} = 20{,}000$ K, $\log g = 4.5$ and log (solar abundance) = 0. The free parameters of the calculation are: $\mu = 1$; $B = 2\,10^4$ G, $\psi = \pi/2$, $\chi = 0$. The reduced intensity $\bar{I} = I(0,\mu)/B_\nu(0)$, where $B_\nu(0)$ is the Planck function at the topmost layer of the truncated model (see the text), $p = \dfrac{Q(0,\mu)}{I(0,\mu)}\,100$ represents the percentage of linear polarization. The full drawn curves correspond to the line formed under the combined Stark-Zeeman effect taking account of thermal motion of the radiators (=using Doppler convolved Stark-Zeeman profile functions). The dashed curves correspond to the case of line formed under the combined Stark-Zeeman effect for the radiators at rest (=using unconvolved Stark-Zeeman profile functions), which are calculated using Mathys' theory of Stark-Zeeman effect. The dotted curves correspond to the case $B \equiv 0$ i.e. pure Stark effect, but the radiator motion being taken into account (=using Doppler convolved Stark profile functions). The line wings reach a continuum level of intensity at $\bar{I} \simeq 2.0$, around 50 Å from the line centre

ever, the following qualitative remarks can be useful in the analysis of hydrogen Zeeman lines.

The dotted curve represents the Hα line profile computed for $B \equiv 0$. The line core is dominated by the Doppler effect. As expected (Mathys, 1985b), the central depth of this non-magnetic line profile is larger than the corresponding magnetic profile (the full line). Further, since the magnetic effects are absent, the line width and the total line strength are smaller than that of magnetic line profile. When $B = 2\,10^4$ G, the Zeeman shift $\Delta\lambda \simeq 0.4$ Å. The Doppler width $\Delta\lambda_D$ on the other hand, varies substantially over the line forming region in the atmosphere. Hence the effect of Doppler convolution is different at different points in the atmosphere. The unconvolved Stark-Zeeman profile functions have a prominent Zeeman peak near $\Delta\lambda = \Delta\lambda_B$. The peak is more pronounced in the case of low electron densities. At higher densities, this peak gradually disappears. This general behaviour of the profile functions is weakly dependent on the temperature. Thus the line shape as well as its width are now mainly determined by the electron density at different levels in the atmosphere. The dashed curves represent the line formation by just the combined Stark-Zeeman effect (viz. without Doppler convolution). The intensity and polarization profiles are nearly similar to a broadened (electronic or resonance) normal Zeeman triplet of a Lorentzian line profile. As mentioned above, the depth variation of the electron density can only change the strength of the peaks at the π and σ positions of the profile function, but not their positions themselves. The shape of the line core region is determined by the magnetic effects and that of wings by the Stark effect. Notice the merging of the non-magnetic Doppler broadened Stark intensity profile (dotted line) with this dashed profile, in the wings. The linear polarization p has peaks at the π and σ components of the Zeeman triplet. This striking similarity to the normal Zeeman pattern is due to the dominance of the magnetic term in the Stark-Zeeman profile function calculation in a strong field (such as $B = 2\,10^4$ G). The wings of the profile are however strongly damped due to the Stark effect, along with ion dynamical contribution to it.

The important case of the line formed under Doppler convolved Stark-Zeeman profile function is shown by the full drawn curves. The intensity profile is significantly broadened due to the Doppler motion of the emitting atoms. The line depth is also larger. The π and σ components are 'Doppler broadened and overlapped' in the convolution process (see Eqs. (13) and (14)), to varying degrees, because of the temperature and electron density gradients in the stellar atmosphere. In other words, the Doppler convolution leads to wide, shallow and flat natured profile function in the deeper layers of the atmosphere, and to centrally peaked and slightly structured (near the Zeeman peaks) profile function in the top layers. But the depth dependence of the Doppler width, and the radiative transfer effect, together lead to a smooth line profile without strong absorption features near the Zeeman components. However, the linear polarization p being a sensitive parameter, manifests itself through Doppler broadened π and σ components.

The magnetic fields encountered in chemically peculiar (CP) stars (or Ap stars) produce magnetic intensification of the lines, which may be nearly a factor of 2 or 3 depending on the field strength being longitudinal or transverse, over large areas on the stellar surface. It is well known that the number densities of absorbing atoms in these atmospheres have to be increased few times, to theoretically match the strength of observed line profiles, if one uses the non-magnetic instead of the Zeeman-split line profiles. The inclusion of Stark effect in the Zeeman line computations can enhance the line strengths significantly, in normally saturated lines such as hydrogen lines. The inclusion of Stark effect in the theoretical computations will have indirect

influence (i) through improved estimation of the surface field strengths and (ii) through the increased line blanketing by hydrogen lines, in the model atmosphere computations. In the case of hydrogen lines formed in magnetic atmospheres, we have to use the Doppler convolved Stark-Zeeman profiles instead of Voigt profiles, in view of the strong linear Stark effect in hydrogen lines, which cannot be depicted fully, by varying the damping constant in a Voigt profile. Also, substantial differences exist between the non-magnetic line profiles (dotted line) and the magnetic line profiles (full line), which implies that, using non-magnetic profiles for matching the observed profiles of magnetic atmospheres may lead to discrepancy.

3. Effect of atomic orientation on Zeeman lines

In a strong magnetic field the atomic magnetic moment is preferentially oriented along the field lines, which results in unequal populations of the Zeeman substates of a given atomic level. This effect is important when the magnetic fields are strong enough to produce full Paschen-Back effect ($B \gg 10^4$ G), but weak enough that the quadratic Zeeman effect can be neglected. Hence the high excitation lines formed in cool ($T_{\rm eff} = 6000$ K) low field ($B \lesssim 10^7$ G) magnetic white dwarfs are significantly affected by this mechanism. It directly affects strengths and depths of Stokes profiles asymmetrically.

In the present calculations we assume that the line is affected only by normal Zeeman effect. An approximate criterion for neglecting the quadratic Zeeman effect is given as $n^4 B_6 \ll 10^4$, where B_6 is the field strength in units of MG ($= 10^6$ G) and n the upper level principal quantum number. In our study we shall employ a field strength of 7.5 MG. The theory of atomic orientation is developed in Pavlov (1975) from which we have taken the relevant formulae. The effect can be easily included in the normal wave or Stokes vector transfer equations. These two formalisms are described in Gnedin and Pavlov (1974). The atomic orientation effect is discussed in Dolginov and Pavlov (1974) and Pavlov (1975). In the conventional notation, the transfer coefficients which include the orientation effect are given by

$$\bar{\eta}_\alpha(\omega) + i\bar{\rho}_\alpha(\omega) = (\eta_\alpha(\omega) + i\rho_\alpha(\omega))[1 - \alpha W] + O(\hbar\omega_c/2kT)^2\,, \tag{16}$$

where

$$W = \frac{\hbar\omega_c}{8\,kT}\,[L(L+1) - L'(L'+1) - 2]; \quad \omega_c = eB/m_e c\,. \tag{17}$$

$\alpha(\Delta m) = 0, \pm 1$ correspond to the p, 1 and r Zeeman components respectively. The coefficients $\bar{\eta}_\alpha(\omega)$ and $\bar{\rho}_\alpha(\omega)$ should be used in place of $\eta_\alpha(\omega)$ and $\rho_\alpha(\omega)$ in the transfer equation described in Nagendra and Peraiah (1985b). The absorption coefficients $\eta_{p,l,r}(\omega)$ and the anomalous dispersion coefficients $\rho_{p,l,r}(\omega)$ are explicitly defined in the same reference. The degree of orientation depends not only on $(\hbar\omega_c/2kT)$, but also on L and L' of the states involved in the transition. W represents the linear perturbation to the dichroic opacities of the non-oriented atoms. Thus the transitions involving high angular momentum states in a low temperature strongly magnetized plasma are affected by atomic orientation, to a large extent. From the equation given above it is clear that $\bar{\eta}_\alpha(\omega) + i\bar{\rho}_\alpha(\omega) \simeq \eta_\alpha(\omega) + i\rho_\alpha(\omega)$ when $\alpha = 0$ which represents the π component of the Zeeman triplet. Also, the σ components are unequally affected, leading to a symmetry breaking of the Stokes vector profiles about the line centre.

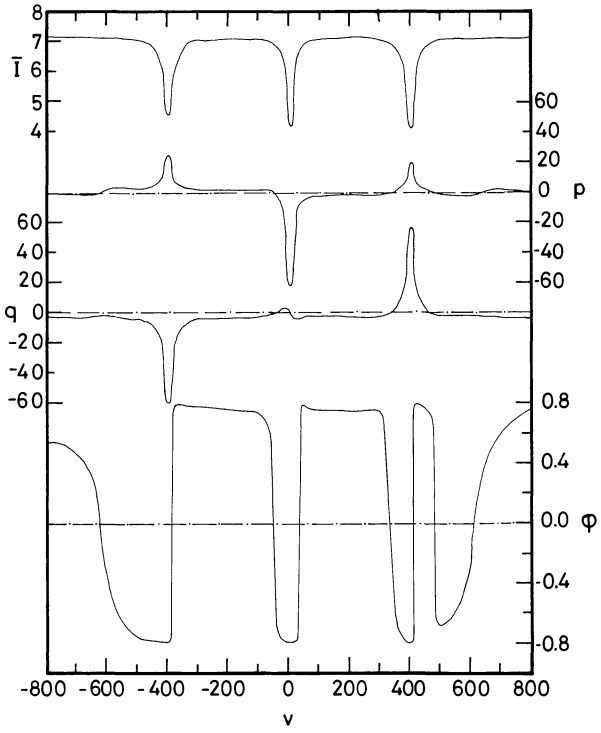

Fig. 2. The variation of the reduced intensity $\bar{I}$, percentage of linear $p = 100 \times (\mathrm{sgn}\,U)\sqrt{Q^2 + U^2}/I$, and circular $q = 100 \times (V/I)$ polarizations as well as the position angle $\varphi = 0.5 \tan^{-1}(U/Q)$ for a Zeeman line when atomic orientation is taken into account. A white dwarf model atmosphere $T_{\rm eff} = 7000$ K, $\log g = 8$, taken from Wehrse (1976) is employed. The following parameters are used: $\eta_0 = 10^4$, $a = 0.1$, $\lambda_0 = 5000$ Å, $\mu = 1$, $\psi = \pi/4$, $\chi = \pi/4$ and a uniform magnetic field of $B = 7.5\,10^6$ G. The continuum is polarized and magneto-optic: $\eta^C_{p,l,r} = 1$, 0.94, 1.1 and $\rho^C_R = -10\cos\psi$, $\rho^C_W = -0.25\sin^2\psi$

In Fig. 2 we have shown the Stokes profiles formed in a magnetic white dwarf atmosphere, computed including this effect. The magnetic dichroism and anomalous dispersion are included in the continuum and the line. The depths of $\bar{I}$, p and q profiles at $v \simeq -400$ are slightly smaller than those at $v \simeq +400$. The position angle being more sensitive, undergoes fluctuations and distortion. When a disk integration is performed, there will be a general reduction in the polarization because of the extreme overlapping of the Zeeman components of the spectral lines. If the strengths of the σ_+ and σ_- components are equal, then such an overlapping leads to large cancellations because of the various orientations and strengths of the magnetic field in the area elements on the visible disk, apart from the usual limb darkening factor which also plays an important role in determining the degree of polarization resulting after disk integration, for a given orientation of the (say) dipole magnetic field. For the same reason mentioned above, the resultant polarization will be relatively larger after a disk integration 'with the orientation effect included', when compared to an identical situation where the atomic orientation is neglected. This is partly due to the unequal strengths of the Zeeman components, their explicit dependence on the orbital quantum number and partly due to the temperature dependence of this effect.

The continuum polarization is quite small for the field strength we have employed (7.5 MG). Still it is nearly 1% in the

far wings. Presently the orientation effect is relatively strong in the line. But, as the field strength increases (~50 to 100 MG), the continuum polarization becomes large and introduces the asymmetries into the line polarization profiles which are more severe than that due to orientation. The atomic orientation itself has to be treated more rigorously than the first order (weak field) treatment presented here. This mechanism is particularly effective in the broadband polarization calculation in magnetic white dwarfs, which have a larger number of Zeeman split spectral lines in a given frequency band.

The atomic orientation thus acts as an additive perturbation along with the continuum polarization, in distorting the components of Zeeman lines, but its contribution becomes insignificant compared to continuum polarization in the case of strong magnetic fields ($B \gtrsim 10^8$ G). The calculation of the continuous dichroic opacities and the solution of the transfer problem in the 'normal wave representation' is described in Nagendra and Peraiah (1985a). The procedure for the same problem in Stokes vector representation is given in Nagendra and Peraiah (1984).

4. The ray refraction effect on the polarization of continuum radiation

The X-ray emission observed in some hot white dwarfs indicates the presence of hot and dense plasma emitting regions near these objects. The examples are Hz 43 and AM Her etc.. A similar situation is encountered in accreting columns of weak field magnetic white dwarfs and neutron stars in binaries. Zheleznyakov (1983) has pointed out that a detailed analysis of the spectra and polarization of these objects in the infrared and radiowave regions of the spectrum is needed in order to understand the accretion mechanisms. In this section we discuss the radiative transfer of far infra-red ($\nu \sim 10^{12}$ Hz) continuum radiation as well as a frequency near the cyclotron resonance occuring in the same spectral range. The refraction effects are included in the calculations. Such infra-red observations are made for an AM Her type star by Bailey et al. (1980). The refractive effects are also important in the calculation of solar radio emission. Thus we believe that whenever the plasma is anisotropic and the refractive indices of normal waves differ significantly from unity, then the ray refraction effects become important.

In this section we use cold plasma normal wave transfer equations. The normal waves (polarization ellipses) remain almost orthogonal away from the cyclotron hormonics and the spectral line centres. The relevant transfer equation for the problem is (see Zheleznyakov, 1970)

$$\mu \frac{dU_j}{d\tau} = \frac{k_j}{k^C}\left[U_j - \frac{B_\nu}{2}\right], \tag{18}$$

where U_j are the modified specific intensities given by

$$U_j = I_j|\cos\alpha_j|/n_j^2, \quad j = 1,2, \tag{19}$$

where α_j, $j = 1,2$ is the angle between the group velocity vector $\mathbf{V}_g$ (direction of the energy flow in a loss free media) and the wave vector of the j^{th} wave. n_j are the real refractive indices, and I_j are usual normal wave ($j = 1$ extraordinary and $j = 2$ ordinary) specific intensities. Clearly, U_j are also (like I_j) the invariants of propagation in an anisotropic refracting medium. Equation (18) holds only within the framework of the approximation of geometrical optics, where the ray treatment is possible. In the case of frequencies away from the cyclotron harmonics, we use analytic expressions given by Zheleznyakov (1970) and Stix (1962), for the cold plasma transfer coefficients α_j, n_j and k_j. Near the cyclotron resonance, the absorption coefficients and the refractive indices of extraordinary and ordinary waves differ from each other by large amounts. Hence we can expect the ray refraction effect on the polarization to be stronger in this region. The cyclotron absorption coefficients for the normal waves ($j = 1,2$) are calculated using the expressions given in Zheleznyakov (1980). The angles α_j are computed now, from the exact relation (Stix, 1962) $\tan\alpha_j = (-1/n_j)\partial n_j/\partial\psi$, since the approximations mentioned earlier are not applicable near the cyclotron resonance. The Faraday rotation of the polarization ellipse with respect to a fixed axis, in the plane, transverse to the propagation direction is given by $\gamma = (1/\omega^2 c)\int_L [\omega_p^2\omega_c\xi dl/(n_1 + n_2)]$ radians, where L is the total geometrical thickness of the plasma slab. $\xi = \cos\psi$ and $\omega_p =$ plasma frequency.

From Table 1, it is seen that the linear (p) and circular (q) polarizations and the Faraday rotation are underestimated if we neglect the ray refraction effect (by taking $n_j \equiv 1$ and $\cos\alpha_j = 1$, $j = 1,2$). The effect is particularly stronger for transverse propagation of the electromagnetic wave, than the longitudinal propagation, with respect to the magnetic field direction. Even in the transverse propagation itself, the error introduced by the neglect of refraction effect, tends to be stronger in a non-uniform magnetic field than in the uniform case. However, the calculation of Faraday rotation in thermal plasmas is not much affected in general, by the neglect of ray refraction effect. From Table 2 it is seen that for frequencies near the cyclotron resonance ω_c the linear and circular polarization show stronger, but qualitatively similar behaviour regarding refraction effect, as in the case of thermal radiation away from the resonance (Table 1). But now, the Faraday rotation decreases when the refractive effects are

Table 1. The difference between the solutions where the refractive effects are included (first column) and neglected (second column) for a uniform magnetic field $B = 10^4$ G. The last two columns show a similar comparison for a field varying as $B(r) = \frac{B_*}{\sqrt{2}}\left(\frac{R_*}{R_* + r}\right)^3$, $B_* = 10^4$ G being the field at the surface ($r = 0$) of a star of radius R_*. The Plasma parameters in both the cases are $T = 10^6$ K; $N_e = 1.65\,10^{14}$ cm^{-3}; $\omega = 6.283\,10^{12}$ Hz and $\mu = 0.8$ and $\psi = 10^0$ (for quasilongitudinal: QL) and $\psi = 72°$ (for quasitransverse: QT) propagations. Total height of the slab is 6 km. p, q and γ represent percentage of linear, circular polarizations and Faraday rotation in radians of the polarization ellipse arising due to propagation

	Uniform field		Non-uniform field	
p_{QL}%	1.31E − 4	1.09E − 4	6.66E − 5	5.56E − 5
q_{QL}%	−3.05E − 1	−2.54E − 1	−2.20E − 1	−1.84E − 1
γ_{QL}	2.33E + 4	2.31E + 4	1.65E + 4	1.64E + 4
p_{QT}%	3.25E − 3	8.50E − 4	2.21E − 3	5.32E − 4
q_{QT}%	−7.93E − 2	−2.07E − 2	−7.66E − 2	−1.84E − 2
γ_{QT}	7.31E + 3	7.26E + 3	5.17E + 3	5.14E + 3

Table 2. Same as Table 1, but for the cyclotron absorption of radiation in a uniform field $B = 3.3\,10^5$ G for an angle of propagation $\psi = 10^0$ (quasilongitudinal: QL). It can be noticed that the error committed in neglecting the refractive effects is enhanced because of the transfer of radiation in optically thick medium

	Uniform field	
$p\%$	1.70E − 2	1.16E − 2
$q\%$	−1.65E + 0	−1.13E + 0
γ	7.65E + 5	8.02E + 5

included (last row of Table 2) because, near the resonance, n_j in particular increase in magnitude unlike the behaviour at a frequency far away from the resonance, where they decrease slightly from the values $n_j \simeq 1$, in the cold plasma theory used here.

It is found that nearly 10% of the observed DA white dwarfs have moderately strong ($B \sim 10^5$ G) and another 5% have weak ($B \sim 10^4$ G) fields. Some among the DC white dwarfs which are generally cool ($T_e \sim 10^4$ K) also have fields in the range 10^4–10^5 G. The existence of thin or extended and hot coronae around the white dwarfs was suggested some time back to explain the wavelength dependent continuum polarization in magnetic white dwarfs (See Landstreet, 1979 for a review). Zheleznyakov (1983) has considered the problem of distortion of the photospheric radiation spectrum of magnetic white dwarfs observed through such dense and hot plasma regions. Recently Greenstein and McCarthy (1985) have employed chromospheric or coronal models, to explain the emission lines in the magnetic white dwarf GD 356. The parameters selected for the study of refraction effects represent such coronae in weak field magnetic white dwarfs. The calculation may also be relevant to the infrared emitting regions or broad line emitting regions near the AM Her type binaries (see Bailey et al., 1980 and Bailey and Ward, 1981). Thus we see that in the solution of normal wave transfer equations, particularly for the long wavelength radiations and near the resonances, the ray refraction effects make significant changes in the polarization over the conventional solutions, obtained neglecting these effects.

5. Conclusions

In the previous sections we have described three mechanisms which are important in a fine analysis of stellar polarization observations. The hydrogen lines formed in early type magnetic stars are largely affected by linear Stark effect. The procedure described in Sect. 2 for computing Stark-Zeeman line profiles, though time consuming for quantitative work, is useful for detailed studies on a particular line. Since these profiles are more sensitive to the electron density, than temperature, they offer a useful tool for estimating that free parameter more accurately. The atomic orientation effect, for the atmospheric and line parameters we have used at present, is very small. Obviously, for high excitation lines formed in cold magnetized plasma regions excited radiatively, this effect is more significant and produces asymmetric Zeeman profiles and contributes to broad band polarizations. The contribution of ray refraction effect to continuum polarization of low frequency radiation propagating in a magnetoplasma is found to be significant. For a frequency near the cyclotron resonance, the Faraday depolarization is effectively decreased in a longitudinal propagation. This aspect may prove useful in the correct calculation of internal Faraday rotation in transparent synchrotron radio sources, by taking the ray refraction effect properly into account.

Acknowledgments. One of us (K.N.N) is grateful to Dr. G. Mathys of Geneva Observatory for providing the complete information required to calculate the results presented in Sect. 2, and for the extremely useful suggestions he made, on all aspects of the calculations presented here. He would also like to thank Dr. G.G. Pavlov for useful comments.

References

Bailey, J., Hough, J.H., Axon, D.J.: 1980, *Nature* **285**, 306
Bailey, J., Ward, M.: 1981, *Monthly Notices Roy. Astron. Soc.* **196**, 425
Cooper, J., Smith, E.W., Vidal, C.R.: 1974, *J. Phys.* **B7**, L101
Dolginov, A.Z., Gnedin, Yu. N., Silant'ev, N.A.: 1970, *J. Quant. Spectrosc. Radiat. Transfer* **10**, 707
Dolginov, A.Z., Pavlov, G.G.: 1974, *Sov. Astron.* **17**, 485
Gnedin, Yu. N., Pavlov, G.G.: 1974, *Sov. Phys-JETP* **38**, 903
Greenstein, J.L., McCarthy, J.K.: 1985, *Astrophys. J.* **289**, 732
Kurucz, R.L.: 1979, *Astrophys. J. Suppl.* **40**, 1
Landstreet, J.D.: 1979, in *White Dwarfs and Variable Degenerate Stars, IAU Coll.* **53**, eds. H.M. Van Horn, V. Weidemann, Univ. Rochester Press, Rochester
Mihalas, D.: 1978, *Stellar Atmospheres*, Freeman, San Francisco
Mathys, G.: 1983, *Astron. Astrophys.* **125**, 13
Mathys, G.: 1984a, *Astron. Astrophys.* **139**, 196
Mathys, G.: 1984b, *Astron. Astrophys.* **141**, 248
Mathys, G.: 1985a, *Astron. Astrophys. Suppl.* **59**, 229
Mathys, G.: 1985b, in *Progress in Stellar Spectral Line Formation Theory*, eds. J.E. Beckman, L. Crivellari, Reidel Dordrecht, p. 381
Nagendra, K.N., Peraiah, A.: 1984, *Astrophys. Space Sci.* **104**, 61
Nagendra, K.N., Peraiah, A.: 1985a, *Monthly Notices Roy. Astron. Soc.* **214**, 203
Nagendra, K.N., Peraiah, A.: 1985b, *Astrophys. Space Sci.* **117**, 121
Nguyen-Hoe., Drawin, H.W., Herman, L.: 1967, *J. Quant. Spectrosc. Radiat. Transfer* **7**, 429
Pavlov, G.G.: 1975, *Astrofiz.* **11**, 77
Smith, E.W., Cooper, J., Vidal, C.R.: 1969, *Phys. Rev.* **185**, 140
Stenflo, J.O.: 1971, in *Solar Magnetic Fields, IAU Symp.* **43**, ed. R. Howard, D. Reidel, Dordrecht, p. 101
Stix, T.H.: 1962, *The Theory of Plasma Waves*, McGraw-Hill, New York
Vidal, C.R., Cooper, J., Smith, E.W.: 1970, *J. Quant. Spectrosc. Radiat. Transfer* **10**, 1011
Vidal, C.R., Cooper, J., Smith, E.W.: 1971, *J. Quant. Spectrosc. Radiat. Transfer* **11**, 263
Wehrse, R.: 1976, *Astron. Astrophys. Suppl.* **24**, 95
Zheleznyakov, V.V.: 1970, *Radio Emission of Sun and Planets*, Pergamon Press, New York
Zheleznyakov, V.V.: 1980, *Astrofiz.* **16**, 316
Zheleznyakov, V.V.: 1983, *Astrophys. Space Sci.* **97**, 229